Aging Effects on the Exciton Relaxation and Diffusion Processes in CsPbBr₃ Nanocrystals

Arianna Cretí, Mauro Lomascolo, Yuhai Zhang, Maria Luisa De Giorgi,
Omar F. Mohammed, and Marco Anni*

Fully inorganic perovskite nanocrystals (NCs) have been widely investigated due to their potential as very interesting active materials for several types of photonic and optoelectronic devices. Despite several experiments designed to investigate the basic emission properties of these NCs, a clear and complete understanding of their photophysics is still missing. In this work, temperature-dependent steady state and time-resolved photoluminescence (PL) measurements are used to investigate the nature of the emitting states, the origin of the excitation relaxation dynamics and the effects of aging upon long exposure to wet air for thin films of CsPbBr₃ NCs prepared by coprecipitation. It is demonstrated that both free excitons and localized excitons contribute to the NC emission and that electron traps within the conduction band, ≈14 meV and ≈80 meV above the band edge, determine thermal emission quenching. Moreover, it is shown that the nonexponential PL relaxation dynamics are due to short-range energy migration within a disordered distribution of localized states between 10 and 100 K, with activation of a second, long-range diffusion process at higher temperatures. It is also demonstrated that aging determines the variations in defect levels, exciton-phonon coupling and exciton relaxation dynamics. The results substantially improve the current understanding of the basic photophysics of CsPbBr₃ NC films and of the aging effects and are expected to provide a useful guide for future characterization of other similar materials.

1. Introduction

Perovskite materials are of great interest in many fields of applications, such as photovoltaic, optoelectronic, and photonic, due to their electronic and optical properties, as well as the low

production costs and ease of processing, which make them very attractive from an industrial point of view. In addition, facile syntheses of lead-halide perovskite nanocrystals (NCs) with controlled size, composition, and shape, which result in wide band gap energy tunability, have further contributed to the rapid increase in research on these materials.[1–6] In particular, fully inorganic NCs (with a typical chemical structure CsPbX₃) show large absorption cross sections,[7] high photoluminescence quantum yields (PLQY),[1,8] high optical gains at room temperature,[9,10] improved stabilities with respect to organic-inorganic NCs,[2] and quantum signatures in their light emission,[7,11,12] which have made it possible to extend the application fields to include photonics[9,10,13,14] and quantum optics.[15,16] The strong application potential of fully inorganic perovskite NCs requires an understanding of their emission properties, of the exciton radiative and non-radiative relaxation processes, of the nature/origin of the emitting states, and consequently of the possible ways to control these properties.

Another very important aspect of understanding lead halide perovskites involves investigations of their interactions with the environment, which typically result in irreversible degradation and lack of long-term stability; that is still the main feature preventing applications in industrial devices.[17–19] Among the

A. Cretí, M. Lomascolo
CNR-IMM
Institute for Microelectronic and Microsystems Unit of Lecce
Via per Monteroni, Lecce 73100, Italy

The ORCID identification number(s) for the author(s) of this article can be found under https://doi.org/10.1002/adom.202202062.

Y. Zhang,[+] O. F. Mohammed
Advanced Membranes and Porous Materials Center Division of Physical Sciences and Engineering
King Abdullah University of Science and Technology
Thuwal 23955-6900, Kingdom of Saudi Arabia

M. L. De Giorgi, M. Anni
Dipartimento di Matematica e Fisica "Ennio De Giorgi"
Università del Salento
Via per Arnesano, Lecce 73100, Italy
E-mail: marco.anni@unisalento.it

[+]Present address: Institute for Advanced Interdisciplinary Research (IAIR), University of Jinan, Shandong 250022, China

different elements leading to perovskite degradation, water and moisture are particularly important and result in irreversible degradation due to decomposition of the active material[17,20] and reversible interactions leading to variations in the emission intensities and lifetimes.[18,21–23] This is particularly important for NC films, which are characterized by larger surface/volume ratios relative to bulk polycrystalline thin films and higher surface defect densities.

In understanding the emission properties of light-emitting materials, investigations of the temperature dependence of photoluminescence (PL) and excitation relaxation dynamics are extremely powerful; they allow us to probe the number of emitting states, their nature (intrinsic or related to defects), coupling with phonons and their energy, and exciton binding energies.[24–29]

For these reasons, several experiments investigating PL temperature dependence have already been performed with fully inorganic NC films, and particular attention been paid to green-emitting $CsPbBr_3$ films that, thanks to the high exciton binding energy of about 40 meV,[1,30–32] show efficient excitonic emission up to room temperature. Interestingly, these experiments did not provide a unique and clear picture of the basic photophysics of these NCs. In particular, despite ample evidence that two different emitting states contribute to the PL spectra of NCs,[22,33,34] the temperature dependence of the spectral features (peak energy, linewidth, intensity, and relaxation dynamics) are always investigated for the entire spectra;[3,34–40] thus, without a detailed investigation of the roles of the two emitting states and their natures, the possibility of ascribing the observed emission properties to the intrinsic properties of the investigated samples is lost.

In addition, the effects of NC aging due to prolonged exposure to (wet) air on the energy levels involved in the emission and on the excitation relaxation dynamics are wholly unexplored.

In this work, we present a detailed optical investigation involving continuous wave (CW) and time-resolved (TR) PL measurements as a function of temperature and determine the nature of the emitting states, the excitation relaxation dynamics, and the effects of aging due to long exposure to wet air (WA) on thin films of $CsPbBr_3$ NCs prepared by coprecipitation. We demonstrate that the PL spectra of the as-deposited film (fresh #F sample) show contributions from two bands, which is attributed to radiative recombination of free excitons (FE) and localized excitons (LE). We show that the temperature-induced intensity quenching of both FE and LE bands is due to thermal activation of two common nonradiative processes, which is ascribed to electron trapping in shallow defect states within the conduction band approximately ≈14 meV and ≈80 meV above the band edge. Moreover, we demonstrate that the PL relaxation dynamics are nonexponential due to short-range energy migration within a disordered distribution of localized states between 10 and 200 K, with activation of a second, long-range diffusion process at higher temperatures.

The same sample after one month of exposure to WA (aged #A sample) showed emission from the same states, but with clear differences in the temperature dependence. We show that aging determined the passivation of electron traps while inducing new hole traps within the valence band at ≈8 meV and

≈120 meV from the band edge. We also demonstrate that aging caused structural changes in the film due to partial NCs aggregation and recrystallization, resulting in variations in exciton–phonon coupling and the characteristics of energy migration.

These results strongly enhance our understanding of the basic photophysics of $CsPbBr_3$ NC films and of the aging effects and are expected to enable the design of novel approaches for development of NCs with properly engineered and optimized optical properties.

2. Results

2.1. PL Spectra

As a first step in understanding the radiative and non-radiative recombination mechanisms for our samples, we performed CW-PL experiments as a function of sample temperature from 10 K up to 290 K (room temperature, RT, in the following). The PL spectra of sample #F at three different representative temperatures (10 K, 150 K, and RT) are provided in **Figure 1**a) and clearly showed multiband line shapes that could be reproduced by superposition of two Gaussian bands.

In particular, at $T = 10$ K, the two bands were centered at 2.330 and 2.355 eV, with full widths at half maximum (FWHM) of ≈70 meV and ≈30 meV, respectively. The spectral position of the narrower peak at higher energy is consistent with the one usually associated in the literature to the free exciton (FE) emission.[3,33,34,37,39,40] Concerning the low energy and broad band, we can exclude any contribution of multiexcitonic species as, in the used pump regime the average number of photons absorbed in each NC is well below 1 (about 0.4). Moreover biexcitons have lower binding energy than excitons,[44] thus they are expected to be thermally dissociated more strongly than the FE as the temperature increases, while our spectra evidence that the low energy peak contribution to the spectra increases as the temperature increases (see Figure S1b, Supporting Information). We then ascribe the low energy emission band to trapped/localized excitons (LE in the following), as previously done in several experiments on the luminescence properties of $CsPbBr3$ NCs films.[33,34,42,43]

As the temperature was increased from 10 K to RT, both bands showed qualitatively similar blue-shifts in peak energy, broadening and intensity quenching, as reported in Figure 1c–e, but with clear quantitative differences.

With regard to the blue-shift, the FE peak energy showed a positive linear increase over the whole temperature range, while the LE band showed a linear shift, with a lower slope, only up to 200 K, followed by clear saturation. These differences determined a progressive increase in the peak energy difference between the two bands (see Figure S1a, Supporting Information), which clearly demonstrated the different natures of the two emitting states.

For the FWHM temperature dependence, the FE band showed broadening from ≈30 meV at 10 K to ≈40 meV at RT, which was much weaker than that of the LE band (from ≈70 meV at 10 K to ≈130 meV at RT).

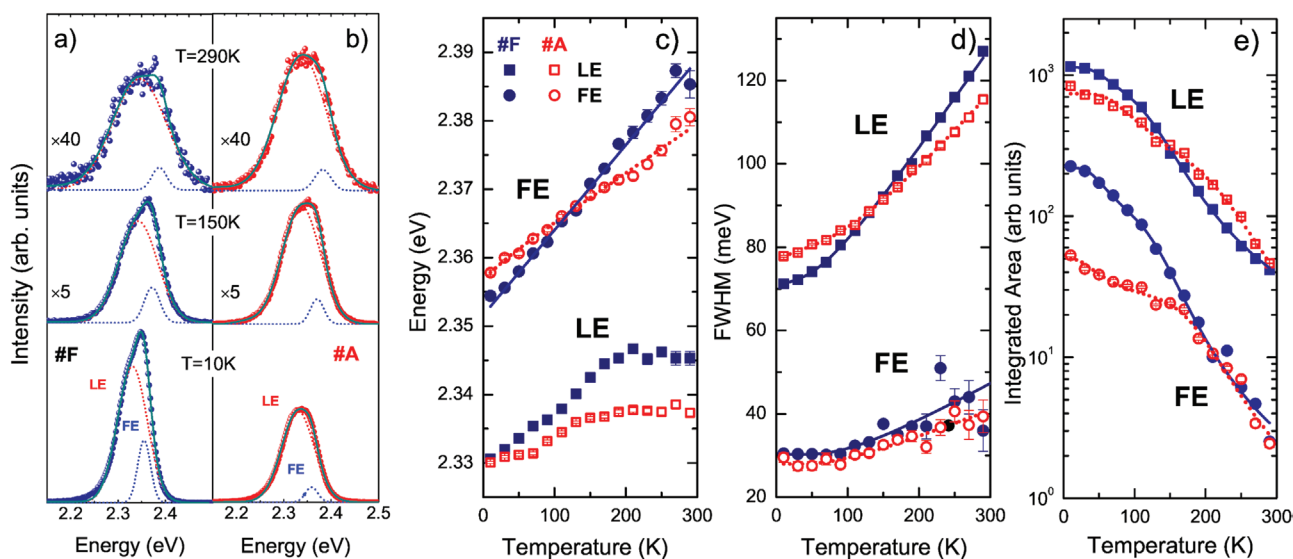Finally, concerning the integrated intensity, progressive quenching was approximately two times stronger for the FE

**ADVANCED
SCIENCE NEWS**

www.advancedsciencenews.com

**ADVANCED
OPTICAL
MATERIALS**

www.advopticalmat.de

Figure 1. a,b) CW-PL emission (symbols) recorded at 10, 150 (×5), and 290 K (×40) for sample #F (a) and sample #A (b), and best fit Gaussian curves. c) Temperature dependence of the LE and FE peak energies for both samples (symbols), and best fit curves with Equation (SI1), Supporting Information. d) Temperature dependence of the FWHM of LE and FE bands for both samples (symbols) and best fit curves with Equation (SI2), Supporting Information. e) Temperature dependence of the integrated area of the LE and FE bands for both samples (symbols) and best fit curves with Equation (1).

band than for the LE band, which resulted in a progressive decrease in the FE relative contribution to the total intensity as the temperature was increased (see Figure S1b, Supporting Information).

We also observe that, as the temperature increases, no further emission bands are observed, evidencing that the observed emission comes from FE and LE in the whole investigated temperature range, without any contribution of other relaxation processes like, for example, free-carriers recombination.

After sample aging, we observed a qualitatively similar PL spectrum (see Figure 1b), which again showed superposition of a narrow peak at high energy and a broad peak at low energy; these were ascribed to FE and LE emissions, respectively. However, a deeper look at the spectra allowed us to observe many differences. In particular, for the data obtained at 10 K, we observed that aging affected the peak energy of the FE band, which was slightly increased, but it did not modify the LE band. In contrast, the FE FWHM was similar to that of sample #F, while the LE FWHM was increased by aging. Finally, the intensities of both bands were reduced by aging, and the relative variation was much stronger for the FE band (approximately fourfold) than for the LE band (≈30%).

Other differences are present in the temperature dependence of all features. In particular, the peak energy blue-shift and the FWHM increase were clearly reduced by aging for both the FE and LE bands (see Figure 1c,d), and LE peak energy saturation took place at a lower temperature (≈150 K) and with a reduced saturation value.

Concerning the band intensity temperature dependence, the FE band of sample #A showed (see Figure 1e) a systematically lower intensity than that of sample #F, but only up to 150 K, and comparable intensities were observed at higher temperatures. Similarly, the LE band showed a lower intensity relative to that for sample #F up to 130 K, a higher intensity at higher

temperatures and an overall comparable intensity at RT. The relative contribution of the FE band to the total emission was basically temperature independent (see Figure S1b, Supporting Information).

Rather curiously, the different temperature dependence seen for the FE and LE band intensities and the different effects of aging on the two bands resulted in comparable total intensities for PL emission at room temperature, thus without any appreciable aging-induced intensity quenching at RT.

To develop a quantitative understanding of the observed features, we performed a best fit of the experimental data with the corresponding model functions.

The experimental temperature-induced PL intensity quenching behavior was reproduced by assuming the superposition of two thermally activated nonradiative processes, which resulted in the following fit function:

$$I(T) = \frac{I_0}{1 + R_1 e^{-\frac{E_{a1}}{kT}} + R_2 e^{-\frac{E_{a2}}{kT}}} \tag{1}$$

where I_0 is the integrated PL intensity at 0 K, k is the Boltzmann constant, E_{ai} ($i = 1, 2$) are the activation energies of nonradiative channels, and R_i the corresponding nonradiative scattering coefficients.

The obtained best fit curves (see Figure 1e) excellently reproduced the experimental data for the best fit values reported in **Table 1**.

The main results are as follows:

i) Two activation energies were required for both the FE and LE bands for both sample #F and sample #A;
ii) The two activation energies of the FE and LE bands in sample #F were comparable within the error bar;[44]
iii) Aging modified the values of the activation energies, which also became different for the FE and LE bands.

Table 1. Best fit activation energies and nonradiative scattering coefficients, and correspondent best fit standard deviation, obtained from the analysis of the temperature induced intensity quenching.

Sample	Peak	R_1	E_{a1} [meV]	R_2	E_{a2} [meV]
#F	FE	5.6 ± 1.4	13.4 ± 1.9	$(1.90 \pm 0.60) \times 10^3$	85.9 ± 5.7
	LE	3.6 ± 1.5	14.8 ± 3.4	$(4.03 \pm 0.88) \times 10^2$	71.1 ± 4.7
#A	FE	1.69 ± 0.53	7.8 ± 3.6	$(1.89 \pm 0.19) \times 10^3$	120 ± 17
	LE	10.4 ± 3.7	25.9 ± 4.4	$(8.58 \pm 0.88) \times 10^3$	166 ± 41

The main results for the temperature dependence of the peak energies and the linewidths of the two bands (see Supporting Information for details on the fit and Figure 1c,d for the best-fit curves) are:

i) The peak energy shift of the FE band of sample #F as a function of temperature was fully ascribed to lattice thermal expansions, without a visible contribution from coupling with LO phonons (see Table S1, Supporting Information);

ii) The peak energy shift of the LE band of sample #F with temperature could not be reproduced with the effects of phonon coupling;

iii) The energy shift reduction of the FE band in sample #A was ascribed to a reduction in the coupling strength with acoustic phonons ($\approx$1.7-fold, see Table S1, Supporting Information);

iv) The linewidth increase of the FE band was mainly due to coupling with LO phonons, without appreciable aging effects (see Table S2, Supporting Information);

v) The linewidth increase of the LE band was instead consistent with a thermally activated broadening, with an activation energy incompatible (at least for the #A sample) with the CsPbBr$_3$ LO phonon energy (see Table S2, Supporting Information).

2.2. PL Relaxation Dynamics

To gain further insight into the exciton relaxation processes and their dependence on sample aging, we also performed TR-PL experiments as a function of temperature between 10 K and RT on both the #F and #A samples. At each temperature, the TR-PL signal was recorded at the maximum of the CW-PL spectrum with a spectral resolution of $\approx$20 meV. Under these experimental conditions, the probed signals resulted from both the FE and LE bands, as the narrower FE emission band was located within the spectrally broadened LE band (see the gray area in the CW-PL spectrum in the inset of **Figure 2**a).

In Figure 2a, we report two representative TR-PL traces for sample #F recorded at 10 K and RT (further data are reported in Figure S2a, Supporting Information); these evidenced clearly non-monoexponential relaxation and became progressively faster as the temperature was increased. In particular, in the early tens of nanoseconds after the laser pulse, the PL exhibited a fast decrease in the signal, followed by a monoexponential decay over longer times.

A non-monoexponential relaxation was also observed for sample #A (see Figure S2b, Supporting Information), which showed a slower initial decay that was more evident at low

temperatures, and a progressively faster decay as the temperature was increased.

Non-monoexponential relaxation is often reported for CsPbBr$_3$ NC films[34,35,45,46] and is typically analyzed with multiexponential decay functions to provide a description of the average lifetime behavior. Even if rather diffuse, this approach is often poorly related to the real photophysics of the investigated sample and neglects the well-known possibility of reasonably reproducing any nonexponential decay with a superposition of a high enough number of exponential decays. In addition, analysis of the average lifetime (whatever it may physically represent) completely eliminates the possibility of investigating individually the different decay processes that cause non-monoexponential relaxation. In our samples, we obtained very good agreement with the experimental data for both samples and at all temperatures by combining three exponential terms that could have a physical basis with three independent decay channels. Since the PL spectra just indicated the presence of two emission bands, we evaluated a triexponential fit unsuitable to reproduce the photophysics of our samples meaningfully (a typical fit output is reported in Figure S3, Supporting Information). We instead investigated the TR-PL data by using a best fit with superimposition of a monoexponential and a stretched exponential decay:[34,47]

$$I(t) = I_0 + C_1 e^{-(t-t_0)/\tau} + C_{st} e^{-((t-t_0)/\tau_{st})^\beta} \qquad (2)$$

where I_0 is the background level, t_0 is the initial time after the system laser response, C_1 and C_{st} are the pre-exponential factors, τ_1 and τ_{st} are the monoexponential and stretched exponential time constants, respectively and β is the stretching factor.

The stretched exponential decay model typically describes the recombination dynamics in complex disordered systems, in which carrier/exciton diffusion and trapping processes play crucial roles, and the value of the stretching factor β is related to the dimensionality of the configuration space wherein the trapping centers are randomly distributed and to the diffusion of excitons toward trap sinks.[34,47–53]

The best-fit curves obtained by using this function properly described the experimental traces at all investigated temperatures and for both samples. The good agreement between the experimental data and the best-fit function is shown in Figure 2a for sample #F at $T = 10$ K, which also shows the contributions of the two components of the decay signal to the total emission intensity as shaded areas (A_1 is related to the monoexponential component and A_{st} is related to the stretched one).

The main features of the best-fit parameter temperature dependence for sample #F are:

i) The monoexponential time constant τ_1 was weakly affected by the temperature and exhibited values of $\approx$90 ns over the whole temperature range (see Figure 2c).

ii) The stretched time constant τ_{st} was constant at $\approx$2.0 ns up to 110 K and then progressively decreases down to about 0.4 ns at RT (see Figure 2c).

iii) The stretching factor β was also basically constant at ≈ 0.6 up to 110 K and then progressively decreased to about 0.4 at RT (see Figure 2d).
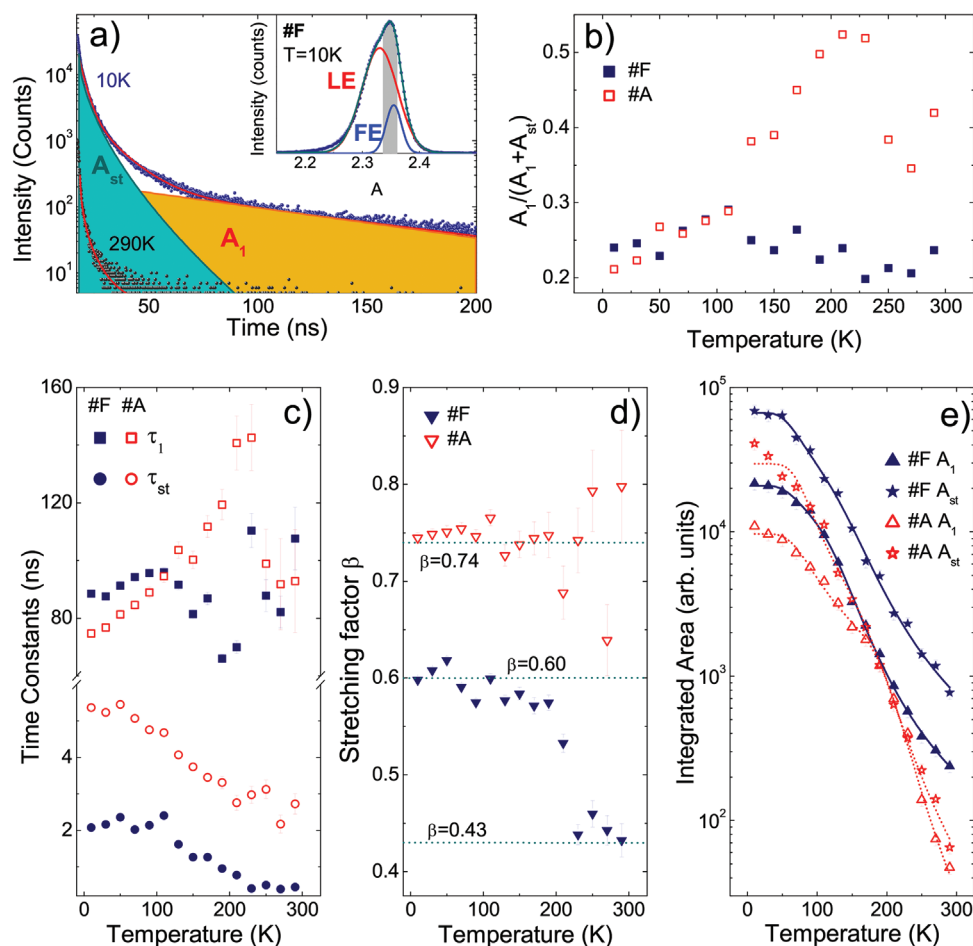
2202062 (4 of 10)

Figure 2. a) TR-PL traces determined at 10 K and RT for sample #F and best fit line of the 10 K signal with Equation (2). The two orange (A_1) and cyan (A_{st}) shadowed area represent the time integrated area under the TR-PL traces of the monoexponential and stretched exponential contributions, respectively. Inset: Spectral range used in TR-PL experiments (colored area) compared with a representative CW-PL spectrum. b) Relative contribution $A_1/(A_1+A_{st})$ of the monomolecular component for samples #F (closed symbols) and #A (open symbols). c,d) Temperature dependence of c) the time constants τ_1 and τ_{st}, and the stretching factor β, for samples #F (closed blue symbols) and #A (open red symbols). e) Temperature dependence of A_1 and A_{st}, for samples #F (closed blue symbols) and #A (open red symbols), and best fit curves with Equation (1).

iv) The time integrated intensities of the two processes showed clear thermally activated progressive decreases, which were quantitatively similar for A_1 and A_{st} (see Figure 2e), with two activation energies comparable with those obtained from the intensity analysis (see **Table 2**).

v) The relative contribution of monoexponential relaxation to the total emission was ≈25% at all the investigated temperatures (see Figure 2b).

Table 2. Best fit activation energies and non-radiative scattering coefficients, and correspondent best fit standard deviation, obtained from the analysis of the PL decay dynamics temperature dependence.

Sample	A_i	R_1	E_{a1} [meV]	R_2	E_{a2} [meV]
#F	A_1	10.1 ± 6.8	22.2 ± 5.7	(2.98 ± 0.62) × 10³	94.6 ± 8.8
	A_{st}	18 ± 11	22.8 ± 5.3	(3.2 ± 1.1) × 10³	95.2 ± 8.6
#A	A_1	27.0 ± 8.4	28.1 ± 3.9	(1.5 ± 1.0) × 10⁶	221 ± 15
	A_{st}	106 ± 62	35.9 ± 6.5	(3.0 ± 2.4) × 10⁵	167 ± 18

After aging, the temperature dependence of the relaxation dynamics was strongly modified, in particular:

i) The mono-exponential time constant τ_1 was reduced at 10 K down to ≈75 ns, but it then increased up to 142 ns at 230 K and then decreased down to ≈92 ns at RT (see Figure 2c).

ii) The stretched time constant τ_{st} increased strongly up to ≈5.5 ns at 10 K and was basically constant up to only 50 K; then, a progressive decrease down to ≈3.5 ns was observed as the temperature was increased up to RT (see Figure 2c).

iii) The stretching factor β also increased up to about 0.74 and became temperature independent up to RT (see Figure 2d).

iv) The contribution of the two processes to the integrated PL intensity still showed a thermally activated progressive decrease with two common activation energies; the overall decrease between 10 K and RT was stronger for A_{st} (see Figure 2e). The activation energies values were comparable (see Table 2), with those extracted from the LE band intensity temperature dependence.

v) The relative contribution of monoexponential relaxation to the total emission was about 20% at $T = 10$ K, and progressively increased up to ≈50% as the temperature was increased (see Figure 2b).

3. Discussion

To relate the previous results to the exciton relaxation processes in our samples, we will start from a proposed energy level scheme that was developed by starting from the activation energies determined from the FE and LE band intensities of both samples. The presence of two thermally activated non-radiative processes was reported in a study of CsPbBr$_3$ NCs prepared by hot injection,[34] in which, despite the evidence that two peaks contributed to the sample emission, only the temperature dependence of the total integrated intensity was analyzed. The two activation energies were basically identical to those of our #F sample (12 ± 3 and 77 ± 18 meV) and were ascribed to thermal detrapping of the FE and LE, respectively. Our separation of the individual emission intensities for the two bands and the evidence that both bands presented two activation energies instead demonstrated that the two activation energies cannot be individually ascribed to the two emission bands; on the contrary, two common thermally activated non-radiative processes are responsible for quenching the intensities of both bands. This can be explained only if the transitions generating the FE and LE bands have a common state (the bottom of the conduction band, assuming that the localization process involves holes, as we will assume in the following, or the top of the valence band if the trapping involves electrons), and the common activation energies are the energies needed to thermally activate depletion of the common state. We thus propose that in sample #F, electron trap states are present within the conduction band at distances of ≈14 and 80 meV from the band edge (see **Figure 3**a).

At low temperature, the top of the conduction band is full (after photoexcitation), thus allowing efficient emission of both FE and LE; as the temperature is increased, thermal induced electrons trapping results in emission quenching for both the FE and LE bands. This is consistent with recent evidence of non-radiative defects within the conduction band of CsPbBr$_3$ NCs.[46,54]

Another novel feature of our results is that the aging effects can be deduced from variations in the activation energies of the two bands, which also become different for FE and LE. This result demonstrates that sample aging strongly affects the energy level scheme. In particular, the activation energy variations indicated that the relative position between the emitting states and the nonradiative state had changed, while the differences between the FE and LE band values clearly demonstrated that the thermally activated transitions no longer involved a common state in the transitions. We thus propose that sample aging had two simultaneous effects: first, it led to passivation of the defect states within the conduction band, which affected the emission of the #F sample and, second, it introduced other traps within the valence band (see Figure 3b). This conclusion is fully consistent with the best fit values for the activation energy, not only qualitatively (the activation energies for the LE bands are higher than those of the FE band because the starting hole level is at higher energy) but also quantitatively. Actually, taking as a reference the activation energies of the FE band and the energy differences between the FE and LE bands (considering a value of ≈30 ± 2 meV observed at low temperature, where the thermally induced exciton redistribution within the localized states is less important), we estimated that the activation energies for the LE band were approximately 38 ± 4 and 150 ± 17 meV (as a simple sum between the FE–LE energy difference and the FE activation energies, with the sum in quadrature of the statistical uncertainty used to determine the error bar). These values were fully compatible, within the statistical error limits, with the LE activation energies of 26 ± 4
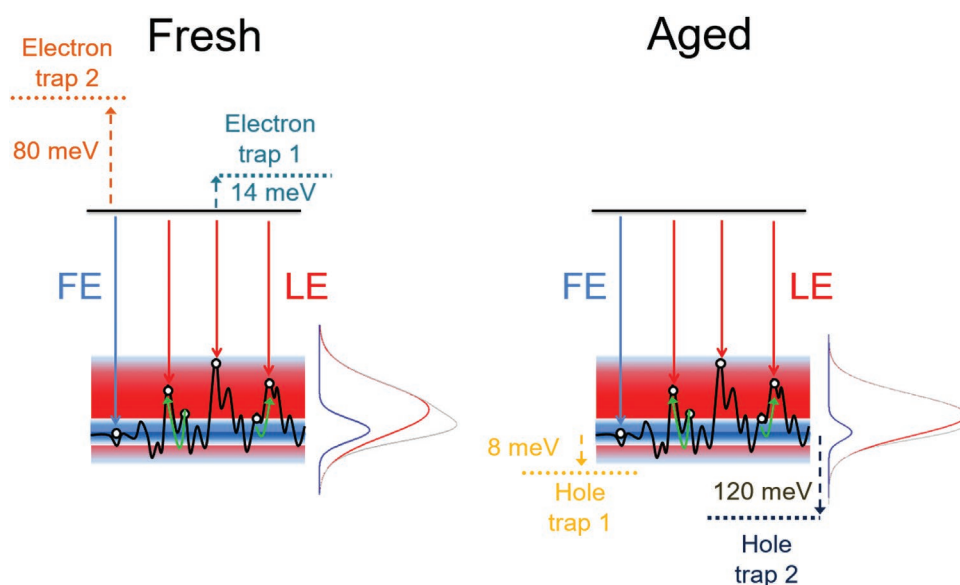

Figure 3. Proposed energy level schemes for samples #F (left) and #A (right). The green arrows indicate energy migration, while the red and blue lines represent the LE and FE radiative recombination, respectively.

2202062 (6 of 10)

**ADVANCED
SCIENCE NEWS**

www.advancedsciencenews.com

**ADVANCED
OPTICAL
MATERIALS**

www.advopticalmat.de

and 170 ± 41 meV obtained from the intensity quenching fits.[44] Overall, our conclusions are also fully consistent with those obtained from an investigation of the environmental effects on the emission properties of $MAPbI_3$ thin films[55] and with the evidence of surface degradation that resulted in formation of new trap states in $CsPbBr_3$ NC films;[20] this allowed us to conclude that all of the observed activation energies for sample #A are related to hole trapping processes. This last conclusion is particularly interesting, as it means that none of the observed activation energies can be related to the exciton binding energy of our NCs, which is widely proposed in the literature[3,35,37,40] without paying particular attention to the widely scattered values of the supposed binding energy in apparently comparable systems, that are inconsistent with the value of an intrinsic property of $CsPbBr_3$. The widely scattered values for PL quenching activation energies are instead fully compatible with an important role for defect trapping, considering the likely sample-to-sample variations in defect energy levels. Our attribution is also fully consistent with recent evidence indicating a correlation between defect density and temperature-induced quenching in $CsPbBr_3$ NCs in solution.[56]

Further insight into the effects of aging on NC properties was provided by the temperature dependence of the FE peak energy, which demonstrated a strong reduction in coupling constants with acoustic phonons (≈40%, see Table S1, Supporting Information). This demonstrated that the aging effect was not only related to passivation and formation of surface defect states but also to a more important material-composition rearrangement, which, although likely involving the surface, also affects the lattice structure by inducing variations in the lattice/bulk behavior of the nanocrystals.

Moving to the exciton relaxation dynamics, our results showed that dispersive energy migration was responsible for PL decay in the first few tens of nanoseconds, while monoexponential relaxation dominated at longer times.

The first aspect to clarify is whether it is possible to individually ascribe the two kinds of relaxation to the FE and LE emissions. A first indication comes from the activation energies, specifically the ones of the integrated contributions of the monoexponential and stretched exponential terms to the total emission. Considering sample #F, the good agreement between the two common activation energies of the FE and LE intensities and of the A_1 and A_{st} activation energies demonstrated that the two observed relaxation processes could be related to the PL emission. However, as the values were largely comparable for both the emission band intensities and for the two relaxation channel integrated intensities, they are not helpful in relating the relaxation dynamics with the FE and LE emission. In contrast, the A_1 and A_{st} activation energies for sample #A are only compatible with those for LE intensity quenching. We can thus conclude that the overall relaxation process reflects relaxation of the LE, without an evident contribution from the FE.

This conclusion is surprising, as one of the decay processes in nonexponential PL decay is always ascribed in the literature to FE radiative recombination;[34,45,46,57] on the other hand, it is fully consistent with the evidence that, within the spectral window probed in the time-resolved measurements, the sample emission was actually dominated by the LE band (see inset of Figure 2a).

A further confirmation that the monoexponential and stretched exponential terms cannot be individually ascribed to FE and LE comes from a comparison between the temperature dependence of the relative LE contribution to the sample emission and the A_1 relative contribution to the sample relaxation. If the monoexponential term was related to FE emission, the two temperature dependencies would be comparable. In contrast, we observed (see Figure S1b, Supporting Information and Figure 2b) that, in sample #F, the FE relative contribution regularly decreased with temperature, while the relative A_1 contribution was almost constant. On the other hand, in sample #A, the FE relative emission was almost constant, while the A_1 relative contribution increased with temperature. Thus, we can conclude that the monoexponential term was not related to radiative recombination of free excitons (as previously proposed in the literature[34]), confirming that also this decay is related to radiative recombination of LE.

Finally, we focus our attention on another very important result provided by fitting the TR-PL signals, which is related to the values of the β stretching factor. Within the theory of diffusion in disordered systems, this parameter is related to the dimensionality of the trap configuration space and to the number of relaxation channels.[48] More explicitly, defining $d^*=fd$, where d is the dimensionality of the configuration space, and f = (number of short range channels)/(number of total channels), diffusion theory predicts $\beta = d^*/(d^* + 2)$. There are some noteworthy values, or *magic values*, of this ratio and, in particular, we highlight the following: i) for $d = 3$ and $f = 1$, thus a single short-range diffusion process within a tridimensional trap distribution, one finds $\beta = 3/5$ (0.60); ii) for $d = 3$ and $f = 1/2$, thus two balanced relaxation channels, one at short-range and one at long-range, one finds $\beta = 3/7 \approx 0.43$.

Starting from the values found for sample #F, we immediately observe that the low and high temperature values exactly corresponded to the two previous *magic values*. The β value of 0.60, found at temperatures below 100 K, is exactly the magic value expected for $d = 3$ and $f = 1$, indicating the presence of a single, short-range diffusion process within a 3D trap distribution. Between 100 and 200 K, β decreased, evidencing a change in the type of migration process, down to $\beta = 0.43$, which is the *magic value* expected for two balanced diffusion processes. We can thus conclude that below 100 K, a single short-range exciton diffusion process is present, while a second one, long-range, is thermally activated at ≈100 K and progressively increases its contribution; this decreases β down to 3/7 above 200 K.

The temperature dependence of the β values is also consistent with the stretched time constant one, evidencing a decrease in the diffusion time when the second process is also thermally activated (see Figure 2c).

The diffusion scenario is strongly modified after aging, as evidenced by the stretching parameter β for sample #A, which assumed a value of ≈0.74 over the whole investigated temperature range. Interestingly, this value does not correspond to any *magic value*, and the variation relative to sample #F is an indication that diffusion and/or relaxation channels have been greatly modified in sample #A. Values of β above 0.6 have been reported in the literature for several other disordered systems.[58] For example, in SiO_2 glasses, a β close to 0.7 was ascribed to combined contributions from values of 0.6

**ADVANCED
SCIENCE NEWS**
www.advancedsciencenews.com
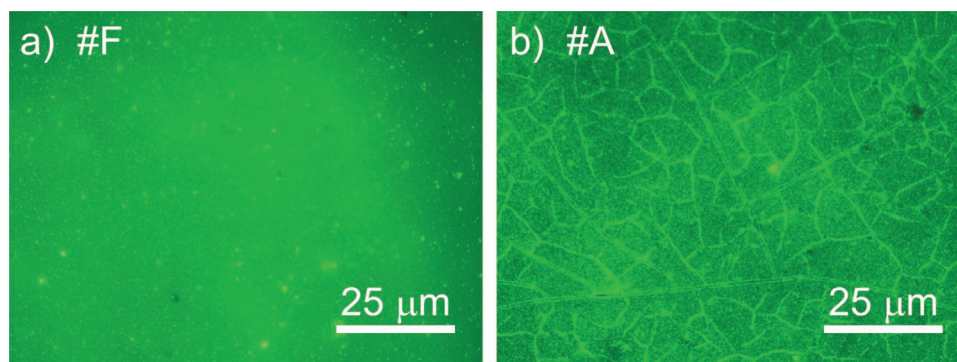
**ADVANCED
OPTICAL
MATERIALS**
www.advopticalmat.de

Figure 4. 220 μm × 160 μm fluorescence map of the samples a) #F and b) #A evidencing the formation of interconnected islands after sample aging.

(disordered glass) and 1 (perfect crystalline glass) due to the coexistence of two nanophases or domains with different crystalline orders.[58] The evidence of exciton diffusion consistent with the presence of mixed crystalline/disordered domains in sample #A strongly validates the hypothesis of material-composition rearrangement, which determined a transition from a random distribution of localized sinks in sample #F to a more ordered distribution in sample #A. This result confirmed that the variations induced by aging impact not only the NC surface and defect passivation/creation, as expected, but also the material bulk, as previously evidenced by variations in the acoustic phonon coupling constant.

The hypothesis of a more homogeneous distribution of trap sinks (lack of random distribution conditions) in sample #A is also consistent with the observed trend for the relative emission contribution of the LE and FE bands, which was independent of T, while a temperature-induced increase in exciton trapping was observed for sample #F (see Figure S1b, Supporting Information).

For the sake of comparison, we observe that our results for the #F sample at room temperature were fully consistent with the β values found for MAPbBr$_3$[47] and CsPbBr$_3$[52] bulk polycrystalline films, evidencing the presence of two diffusion processes in these films. In contrast, the low-temperature β value of 0.6 is clearly different from that of the CsPbBr$_3$[52] bulk polycrystalline film ($\approx$0.73), indicating that a short-range exciton diffusion process was only visible in NC films, while mixed crystalline/disordered domains were present when solution processes were used to prepare bulk polycrystalline thin films.

Concerning the results obtained for CsPbBr$_3$ NCs realized by hot-injection,[34] we instead found similar values of $\approx$0.6 at low temperatures but then saw a decrease down to 0.43 instead of an increase up to $\approx$0.71. This different temperature dependence was consistent with the higher relative LE/FE intensities in our samples, which confirmed that the coprecipitation growth method led to formation of NCs with a higher density of bromine vacancies on the surface compared to NCs grown by hot injection,[22] and thus to a more evident role for exciton localization in the PL relaxation dynamics.[59]

To directly confirm aging-induced formation of crystalline domains in sample #A, we also performed photoluminescence mapping measurements with the two samples. The obtained maps showed that sample #F (see **Figure** 4a) had a generally uniform morphology with a few micrometric regions exhibiting

brighter emission, which indicated NCs aggregation. The #A sample morphology was instead very different (see Figure 4b) and showed evidence for formation of interconnected islands with typical lateral sizes of a few tens of microns; this demonstrated NCs aggregation and recrystallization of the film. Such variations are likely related to NCs surface degradation, which allowed NCs coalescence and growth of larger bulk-like domains giving rise to a partial NC$\rightarrow$ bulk film transition similar to that recently observed after film heating.[60]

Finally, in order to have a direct insight into the eventual NCs aging induced coalescence we also performed TEM measurements, thus probing the NCs shape and size both for fresh NCs and for aged ones. It should be noted that the one-month aging was performed in the solid state of NC film. To take a TEM image, the aged film was rinsed by cyclohexane to redisperse the NCs before drop casting on TEM grid. The obtained results (see Figure S4a,b, Supporting Information) allowed us to observe that the fresh NCs have a rectangular shape, with average diagonal length of 15 ± 8 nm. After the aging process (see Figure S4c,d, Supporting Information), the rectangular shape is preserved, but the NCs size is considerably increased up to 80 ± 25 nm, thus clearly confirming that NCs coalescence takes place due to the NCs aging.

On the contrary, no evident variations of the XRD spectra are observed after aging (see Figure S5, Supporting Information), with spectra dominated by diffraction peaks at 7.7° and 11.5°, that are signature of NCs self-assembly with an interplane spacing of 3.8° (2.2 nm), not affected by the aging,[61,62] and a broad peak at 15.6° suggesting a mixed phase of CsPbBr$_3$ with both cubic and orthorhombic in both samples, with a decreased content of the latter in the aged sample.

The evidence of energy migration affecting the LE emission also allows to understand the different temperature dependence of the peak energy and the FWHM of the FE and LE peaks. FE emission has a temperature dependence affected by the temperature dependence of intrinsic states, thus a peak energy shifting with temperature due to the temperature dependence of the energy gap, and a linewidth increasing due to the increasing contribution of exciton LO-phonon interaction. On the contrary, LE emission is also affected by the temperature dependence of the energy migration.[63] At low temperature, when the thermal energy is lower than the average energy distance between close localized states, the localized excitons migrate toward local minima of the energy distribution. In this temperature range the

peak energy basically follow the intrinsic bands one (assuming a temperature independent relative position in energy of the localized states with respect to the intrinsic ones). As the temperature increases, the increased thermal energy also allows energy migration toward higher-lying localized states (up-hill energy migration), that allows the excitons to reach deeper minima. The energy distribution of the localized excitons thus progressively shifts toward the low energy tail of the localized states distribution. This interplay between blue-shift of the intrinsic states and increasing red-shift due to increasing energy migration toward low energy states, determines a weaker blue-shift of the LE peak energy, up to a regime in which the two shifts are of comparable strength, thus determining the observed saturation. The aging induced transition toward a more uniform distribution of localized states determines a higher role of the energy migration contribution to the shift, thus leading to a weaker shift in temperature and a saturation at lower temperature.

Concerning the temperature dependence of the LE peak FWHM, the observed stronger increase with respect to the FE peak is consistent with the combined contribution of exciton–phonon coupling and, in addition, of a progressive increase of the probability to thermally reach the high energy tail of the localized states distribution, as the temperature increases.

4. Conclusion

In conclusion, we investigated the origins of the emitting states and excitation relaxation processes in $CsPbBr_3$ NC thin films. Our results demonstrated that both FE and LE excitons contribute to sample emission and that PL thermal quenching is due to thermally activated trapping by shallow defects within the conduction band. We also demonstrated that sample aging upon long exposure to WA passivated these traps while inducing the formation of hole traps within the valence band. We also demonstrated that nonexponential PL relaxation is due to energy migration within a disordered distribution of localized states, with temperature- and aging-dependent features. Our results and our data analyses improve the current understanding of the basic photophysics and aging effects of $CsPbBr_3$ NCs and are expected to aid future development of NCs with optimized emission properties.

5. Experimental Section

Sample Preparation: The $CsPbBr_3$ NCs were synthesized by a coprecipitation method, as described in detail in ref. [22]. The thin film was prepared by drop casting on a glass substrate and showed a PLQY of 88%, evidencing the high optical quality of the NCs. The measurements were performed both on an as-deposited film (sample #F) and after aging of one month (sample #A). The performed aging simulated a simple exposure to ambient air, and it had been performed by leaving for 30 days the fresh sample exposed to ambient air, in dark, in a laboratory with controlled temperature and humidity (average temperature 19 °C and average relative humidity 50%).

Characterization: TEM images were collected by a transmission electron microscope (JEM-1400, JEOL) under an acceleration voltage of 120 kV.

Powder X-ray diffraction (XRD) patterns were recorded with an X-ray diffractometer (SmartLab SE, Rigaku) coupled with Cu-Kα radiation ($\lambda = 1.5406$ Å) at room temperature.

PL and TR-PL measurements were performed by exciting the samples by a solid-state pulsed laser (mod. PLP-10, Hamamatsu), which provided pulses at a wavelength of 400 nm for ≈58 ps, at repetition rate of 1 MHz, and s maximum peak power of ≈70 mW. In the time-resolved measurements, the PL was dispersed by an iHR320 (focal length of 0.32 m) Horiba monochromator equipped with a Peltier cooled Hamamatsu photomultiplier (Head-on mod R943-02) operating in single photon counting mode. The TR-PL measurements were performed by time-correlated single photon counting (TCSPC) with an Edinburg Instruments TCC900 TSCPC electronics card. The temporal response of the system to the laser pulse was 0.46 ns. The CW-PL signal was collected in the backscattering configuration by an optical fiber (diameter 1 mm) and dispersed by a Triax320 (focal length of 0.32 m) Jobin–Yvon monochromator coupled to a Peltier cooled CCD. The PL and TR-PL experiments were performed within the temperature range 10 K to 300 K by putting the samples on the cold finger of a helium closed-cycle cryostat.

The PL mapping measurements were performed by a Nikon Eclipse C1 fluorescence inverted microscope, with a 40× objective. The samples were excited in the 470–490 nm range with a Hg lamp and the PL collected in the 520–560 nm range and detected with a CCD. The excitation and collection spectral ranges were selected with bandpass dielectric filters.

Supporting Information

Supporting Information is available from the Wiley Online Library or from the author.

Conflict of Interest

The authors declare no conflict of interest.

Data Availability Statement

The data that support the findings of this study are available from the corresponding author upon reasonable request.

[1] L. Protesescu, S. Yakunin, M. I. Bodnarchuk, F. Krieg, R. Caputo, C. H. Hendon, R. X. Yang, A. Walsh, M. V. Kovalenko, *Nano Lett.* **2015**, *15*, 3692.

[2] F. Krieg, S. T. Ochsenbein, S. Yakunin, S. ten Brinck, P. Aellen, A. Süess, B. Clerc, D. Guggisberg, O. Nazarenko, Y. Shynkarenko,

S. Kumar, C.-J. Shih, I. Infante, M. V. Kovalenko, *ACS Energy Lett.* **2018**, *3*, 641.

[3] H. Yang, Y. Zhang, J. Pan, J. Yin, O. M. Bakr, O. F. Mohammed, *Chem. Mat.* **2017**, *29*, 8978.

[4] S. Wei, Y. Yang, X. Kang, L. Wang, L. Huang, D. Pan, *Chem. Commun.* **2016**, *52*, 7265.

[5] F. Zhang, H. Zhong, C. Chen, X.-g. Wu, X. Hu, H. Huang, J. Han, B. Zou, Y. Dong, *ACS Nano* **2015**, *9*, 4533.

[6] S. Sarkar, V. K. Ravi, S. Banerjee, G. R. Yettapu, G. B. Markad, A. Nag, P. Mandal, *Nano Letters* **2017**, *17*, 5402.

[7] F. Hu, H. Zhang, C. Sun, C. Yin, B. Lv, C. Zhang, W. W. Yu, X. Wang, Y. Zhang, M. Xiao, *ACS Nano* **2015**, *9*, 12410.

[8] F. Liu, Y. Zhang, C. Ding, S. Kobayashi, T. Izuishi, N. Nakazawa, T. Toyoda, T. Ohta, S. Hayase, T. Minemoto, K. Yoshino, S. Dai, Q. Shen, *ACS Nano* **2017**, *11*, 10373.

[9] S. Yakunin, L. Protesescu, F. Krieg, M. I. Bodnarchuk, G. Nedelcu, M. Humer, G. De Luca, M. Fiebig, W. Heiss, M. V. Kovalenko, *Nat. Commun.* **2015**, *6*, 8056.

[10] M. L. De Giorgi, F. Krieg, M. V. Kovalenko, M. Anni, *Sci. Rep.* **2019**, *9*, 17964.

[11] Y.-S. Park, S. Guo, N. S. Makarov, V. I. Klimov, *ACS Nano* **2015**, *9*, 10386.

[12] G. Rainó, G. Nedelcu, L. Protesescu, M. I. Bodnarchuk, M. V. Kovalenko, R. F. Mahrt, T. Stöferle, *ACS Nano* **2016**, *10*, 2485.

[13] M. Ahmadi, T. Wu, B. Hu, *Adv. Mater.* **2017**, *29*, 1605242.

[14] B. R. Sutherland, E. H. Sargent, *Nat. Photonics* **2016**, *10*, 295.

[15] G. Rainò, M. A. Becker, M. I. Bodnarchuk, R. F. Mahrt, T. Kovalenko, M. V. Kovalenko, T. Stöferle, *Nature* **2018**, *563*, 671.

[16] H. Utzat, W. Sun, A. E. K. Kaplan, F. Krieg, M. Ginterseder, B. Spokoyny, N. D. Klein, K. E. Shulenberger, C. F. Perkinson, M. V. Kovalenko, M. G. Bawendi, *Science* **2019**, *363*, 1068.

[17] S. Cheng, H. Zhong, *J. Phys. Chem. Lett.* **2022**, *13*, 2281.

[18] Y. Wei, Z. Cheng, J. Lin, *Chem. Soc. Rev.* **2019**, *48*, 310.

[19] Z. Shangguan, X. Zheng, J. Zhang, W. Lin, W. Guo, C. Li, T. Wu, Y. Lin, Z. Chen, *Nanomaterials* **2020**, *10*, 7.

[20] S. Huang, Z. Li, B. Wang, N. Zhu, C. Zhang, L. Kong, Q. Zhang, A. Shan, L. Li, *ACS Appl. Mat. Interfaces* **2017**, *9*, 7249.

[21] I. Enomoto, Y. Iso, T. Isobe, *J. Mater. Chem. C* **2022**, *10*, 102.

[22] M. Anni, A. Cretí, Y. Zhang, M. L. De Giorgi, M. Lomascolo, *Appl. Sci.* **2020**, *10*, 6.

[23] M. Lorenzon, L. Sortino, Q. Akkerman, S. Accornero, J. Pedrini, M. Prato, V. Pinchetti, F. Meinardi, L. Manna, S. Brovelli, *Nano Lett.* **2017**, *17*, 3844.

[24] C. S. Ponseca, T. J. Savenije, M. Abdellah, K. Zheng, A. Yartsev, T. Pascher, T. Harlang, P. Chabera, T. Pullerits, A. Stepanov, J.-P. Wolf, V. Sundström, *J. Am. Chem. Soc.* **2014**, *136*, 5189.

[25] K. P. Goetz, A. D. Taylor, F. Paulus, Y. Vaynzof, *Adv. Funct. Mater.* **2020**, *30*, 1910004.

[26] T. Kirchartz, J. A. Marquez, M. Stolterfoht, T. Unold, *Adv. Energy Mater.* **2020**, *10*, 1904134.

[27] Y. Wu, R. Jia, J. Xu, L. Song, Y. Liu, Y. Zhang, S. Ullah, J. Dai, *Front. Mater.* **2022**, *9*, 845977.

[28] A. Manoli, P. Papagiorgis, M. Sergides, C. Bernasconi, M. Athanasiou, S. Pozov, S. A. Choulis, M. I. Bodnarchuk, M. V. Kovalenko, A. Othonos, G. Itskos, *ACS Appl. Nano Mater.* **2021**, *4*, 5084.

[29] M. Anni, A. Cretí, M. L. De Giorgi, M. Lomascolo, *Nanomaterials* **2021**, *11*, 6.

[30] Q. Zhang, R. Su, X. Liu, J. Xing, T. C. Sum, Q. Xiong, *Adv. Funct. Mater.* **2016**, *26*, 6238.

[31] Y. Wang, H. Sun, *Small Methods* **2018**, *2*, 1700252.

[32] Y. Wang, Y. Ren, S. Zhang, J. Wu, J. Song, X. Li, J. Xu, C. H. Sow, H. Zeng, H. Sun, *Commun. Phys.* **2018**, *1*, 96.

[33] S. M. Lee, C. J. Moon, H. Lim, Y. Lee, M. Y. Choi, J. Bang, *J. Phys. Chem. C* **2017**, *121*, 26054.

[34] A. Dey, P. Rathod, D. Kabra, *Adv. Opt. Mater.* **2018**, *6*, 1800109.

[35] J. Li, X. Yuan, P. Jing, J. Li, M. Wei, J. Hua, J. Zhao, L. Tian, *RSC Adv.* **2016**, *6*, 78311.

[36] J. Li, L. Wang, X. Yuan, B. Bo, H. Li, J. Zhao, X. Gao, *MRS Bull.* **2018**, *102*, 86.

[37] X. Yuan, X. Hou, J. Li, C. Qu, W. Zhang, J. Zhao, H. Li, *Phys. Chem. Chem. Phys.* **2017**, *19*, 8934.

[38] B. T. Diroll, G. Nedelcu, M. V. Kovalenko, R. D. Schaller, *Adv. Funct. Mater.* **2017**, *27*, 1606750.

[39] B. T. Diroll, H. Zhou, R. D. Schaller, *Adv. Funct. Mater.* **2018**, *28*, 1800945.

[40] X. Zhang, G. Pang, G. Xing, R. Chen, *Mater. Today Phys.* **2020**, *15*, 100259.

[41] K. Shulenberger, M. N. Ashner, S. K. Ha, F. Krieg, M. V. Kovalenko, W. A. Tisdale, M. G. Bawendi, *J. Phys. Chem. Lett.* **2019**, *10*, 5680.

[42] X. Lao, Z. Yang, Z. Su, Z. Wang, H. Ye, M. Wang, X. Yao, S. Xu, *Nanoscale* **2018**, *10*, 9949.

[43] M. Nikl, K. Nitsch, E. Mihakova, K. Polak, G. Pazzi, M. Gurioli, S. Santucci, R. Phani, A. Scacco, F. Somma, *Phys. E* **1999**, *4*, 323.

[44] In order to evaluate the compatibility of two values we determined their difference, and its statistical error bar (calculated as square root of the sum in quadrature of the statistical error bar of each value). The values are considered compatible if the difference is smaller than three times the statistical error.

[45] H. Chen, A. Guo, J. Zhu, L. Cheng, Q. Wang, *Appl. Surf. Sci.* **2019**, *465*, 656.

[46] M. Liao, B. Shan, M. Li, *J. Phys. Chem. C* **2021**, *125*, 21062.

[47] H. He, Q. Yu, H. Li, J. Li, J. Si, Y. Jin, N. Wang, J. Wang, J. He, X. Wang, Y. Zhang, Z. Ye, *Nat. Commun.* **2016**, *7*, 10896.

[48] J. Phillips, *J. Non-Cryst. Solids* **2011**, *357*, 3853.

[49] S. F. Chichibu, T. Onuma, T. Aoyama, K. Nakajima, P. Ahmet, T. Chikyow, T. Sota, S. P. DenBaars, S. Nakamura, T. Kitamura, Y. Ishida, H. Okumura, *J. Vac. Sci. Technol., B: Microelectron. Process. Phenom.* **2003**, *21*, 1856.

[50] Y. J. Sun, O. Brandt, S. Cronenberg, S. Dhar, H. T. Grahn, K. H. Ploog, P. Waltereit, J. S. Speck, *Phys. Rev. B* **2003**, *67*, 041306.

[51] T. Onuma, A. Chakraborty, B. A. Haskell, S. Keller, S. P. DenBaars, J. S. Speck, S. Nakamura, U. K. Mishra, T. Sota, S. F. Chichibu, *Appl. Phys. Lett.* **2005**, *86*, 151918.

[52] C. Wolf, T.-W. Lee, *Mater. Today Energy* **2018**, *7*, 199.

[53] D. C. Johnston, *Phys. Rev. B* **2006**, *74*, 184430.

[54] S. Mandal, S. Mukherjee, C. K. De, D. Roy, S. Ghosh, P. K. Mandal, *J. Phys. Chem. Lett.* **2020**, *11*, 1702.

[55] R. Brenes, D. Guo, A. Osherov, N. K. Noel, C. Eames, E. M. Hutter, S. K. Pathak, F. Niroui, R. H. Friend, M. S. Islam, H. J. Snaith, V. Bulović, T. J. Savenije, S. D. Stranks, *Joule* **2017**, *1*, 155.

[56] Q. Zhang, Z. Li, M. Liu, L. Kong, W. Zheng, B. Wang, L. Li, *J. Phys. Chem. Lett.* **2020**, *11*, 993.

[57] N. Kumawat, A. Swarnkar, A. Nag, D. Kabra, *J. Phys. Chem. C* **2018**, *122*, 13767.

[58] J. C. Phillips, *Rep. Prog. Phys.* **1996**, *59*, 1133.

[59] D. Yang, X. Li, Y. Wu, C. Wei, Z. Qin, C. Zhang, Z. Sun, Y. Li, Y. Wang, H. Zeng, *Adv. Opt. Mater.* **2019**, *7*, 1900276.

[60] R. A. Scheidt, C. Atwell, P. V. Kamat, *ACS Mater. Lett.* **2019**, *1*, 8.

[61] L. Wang, K. Fu, R. Sun, H. Lian, X. Hu, Y. Zhang, *Nano-Micro Lett.* **2019**, *11*, 52.

[62] R. Sun, Z. Wang, H. Wang, Z. Chen, Y. Yao, H. Zhang, Y. Gao, X. Hao, H. Liu, Y. Zhang, *ACS Appl. Mat. Interf.* **2022**, *14*, 36801.

[63] M. Anni, M. E. Caruso, S. Lattante, R. Cingolani, *J. Chem. Phys.* **2006**, *124*, 134707.